# Covalent mechanochemical functionalization of carbon-encapsulated iron nanoparticles towards improvement of their colloidal stability

## Electronic Supplementary Information (ESI)

Artur Kasprzak[a]*, Kristina Fateyeva[a], Michał Bystrzejewski[b], Waldemar Kaszuwara[c], Maciej Fronczak[b], Mariola Koszytkowska-Stawinska[a], and Magdalena Poplawska[a]

*corresponding author e-mail: akasprzak@ch.pw.edu.pl

[a] Faculty of Chemistry, Warsaw University of Technology, Noakowskiego Str. 3, 00-664 Warsaw, Poland

[b] Faculty of Chemistry, University of Warsaw, Pasteura Str. 1, 02-093 Warsaw, Poland

[c] Faculty of Materials Science, Warsaw University of Technology, Wołoska Str. 141, 02-507 Warsaw, Poland

## 1. FT-IR spectra

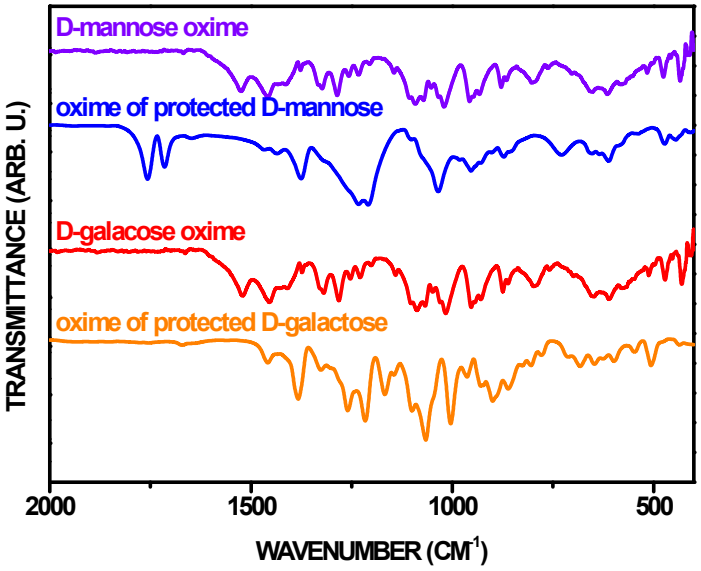


***Fig. S1.*** FT-IR spectra of the sugar oximes

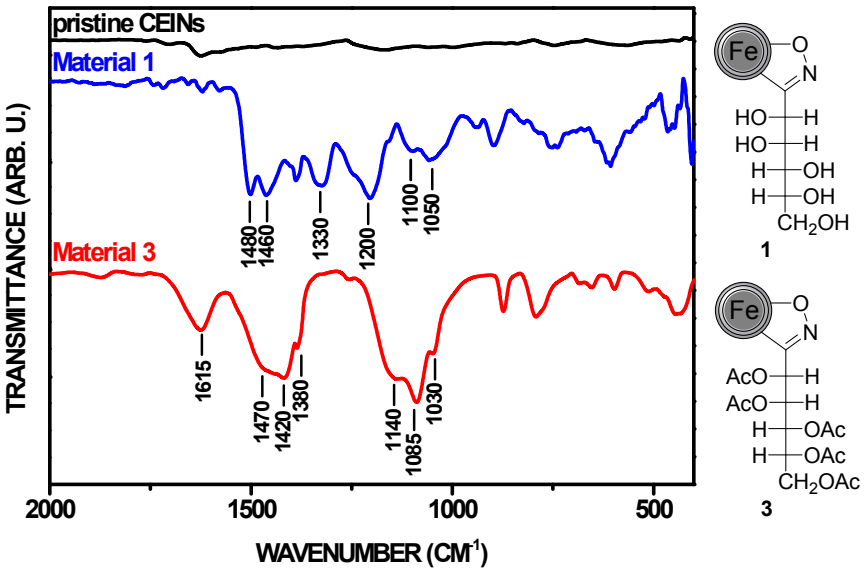


***Fig. S2.*** FT-IR spectra of materials **1** and **3**. FT-IR spectrum of pristine CEINs is also presented.

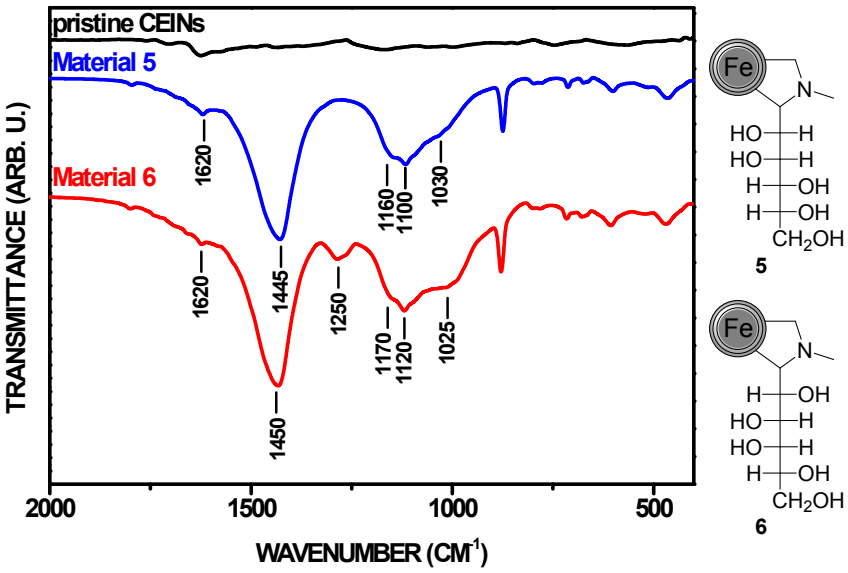


***Fig. S3.*** FT-IR spectra of materials **5** and **6**. FT-IR spectrum of pristine CEINs is also presented.

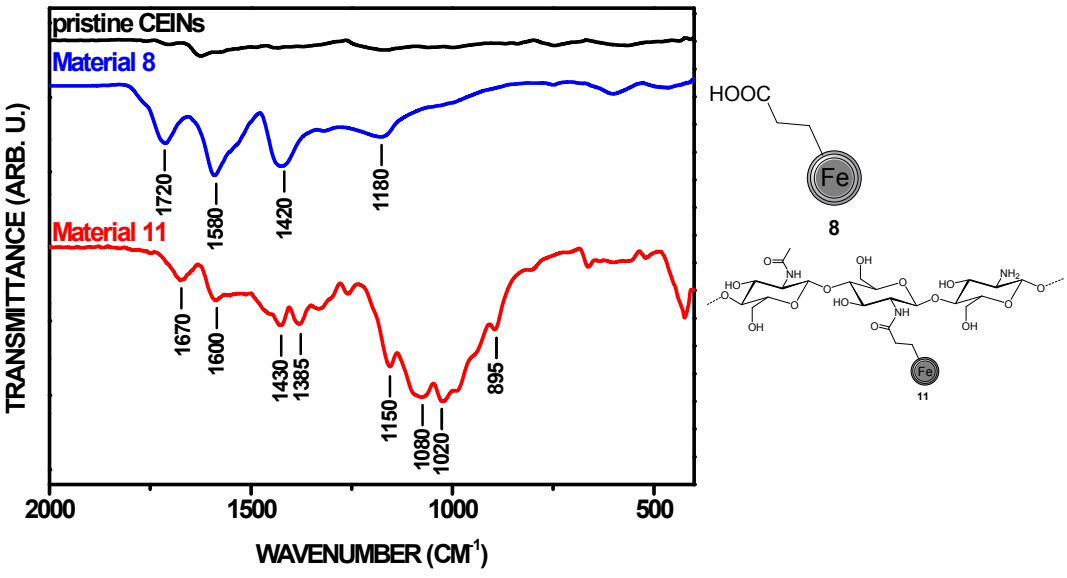


***Fig. S4.*** FT-IR spectrum of material **11**. FT-IR spectra of pristine CEINs and CEINs-$(CH_2)_2$-COOH (**8**) are also presented.

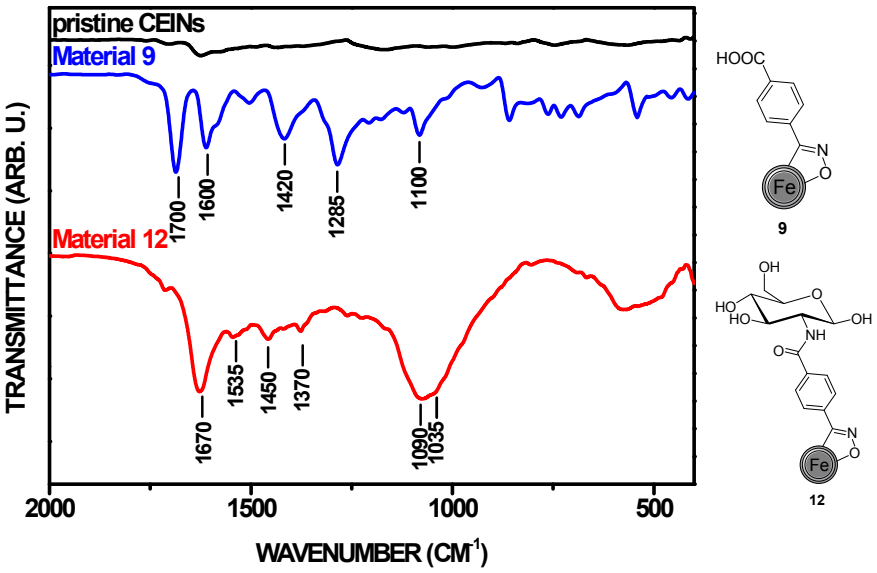


***Fig. S5.*** FT-IR spectrum of material **12**. FT-IR spectra of pristine CEINs and CEINs-isoxazoline-COOH (**9**) are also presented.

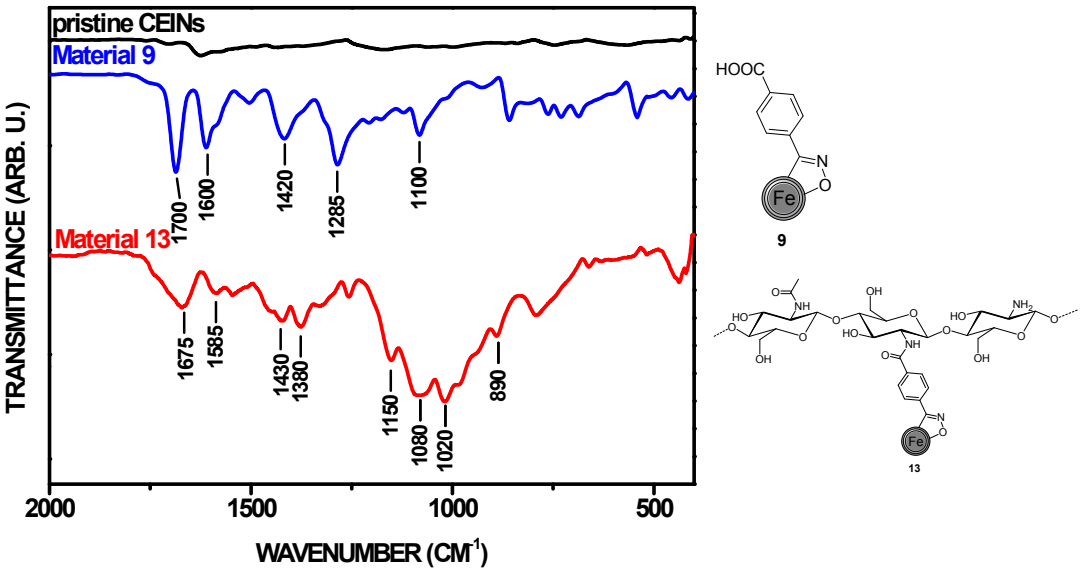


***Fig. S6.*** FT-IR spectrum of material **13**. FT-IR spectra of pristine CEINs and CEINs-isoxazoline-COOH (**9**) are also presented.

## 2. TEM images

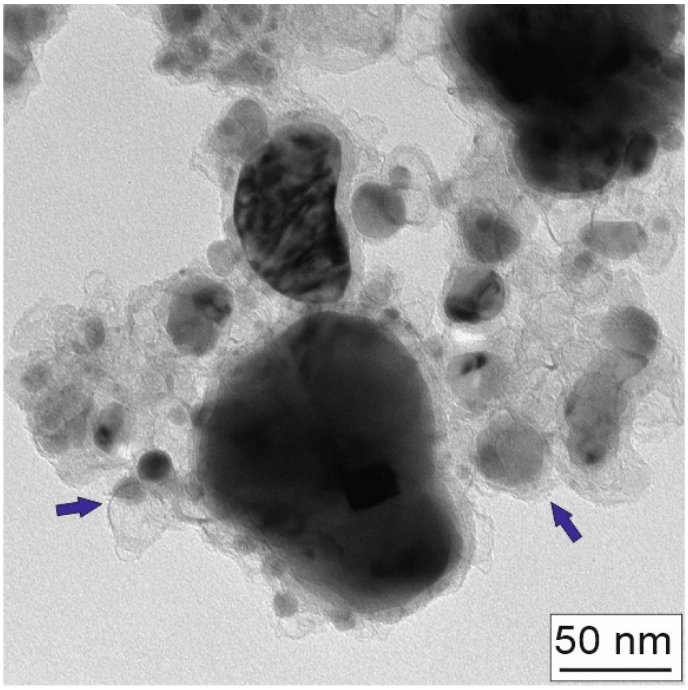


***Fig. S7.*** Representative TEM image of material **2**.

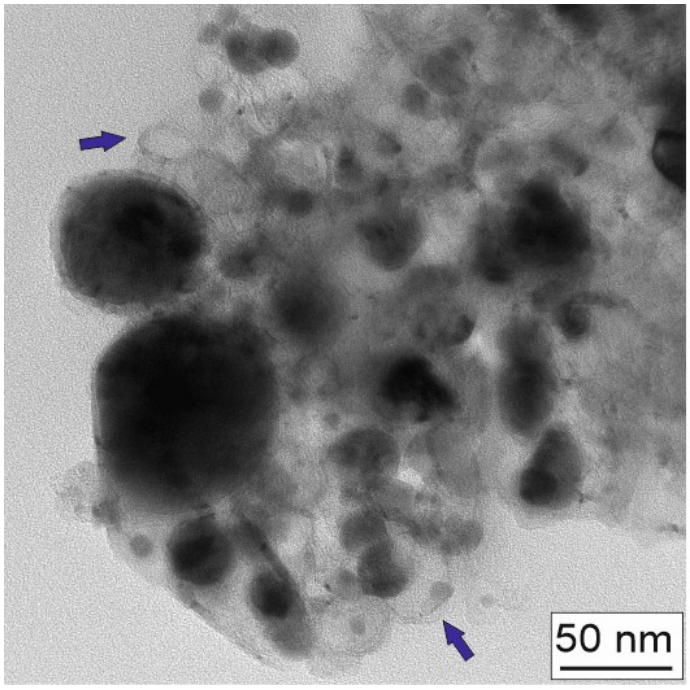


***Fig. S8.*** Representative TEM image of material **4**.

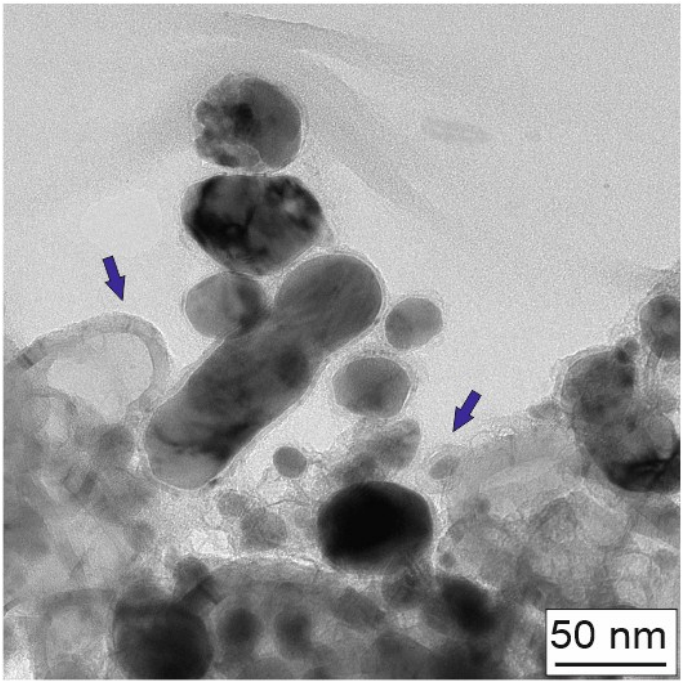


***Fig. S9.*** Representative TEM image of material **5**.

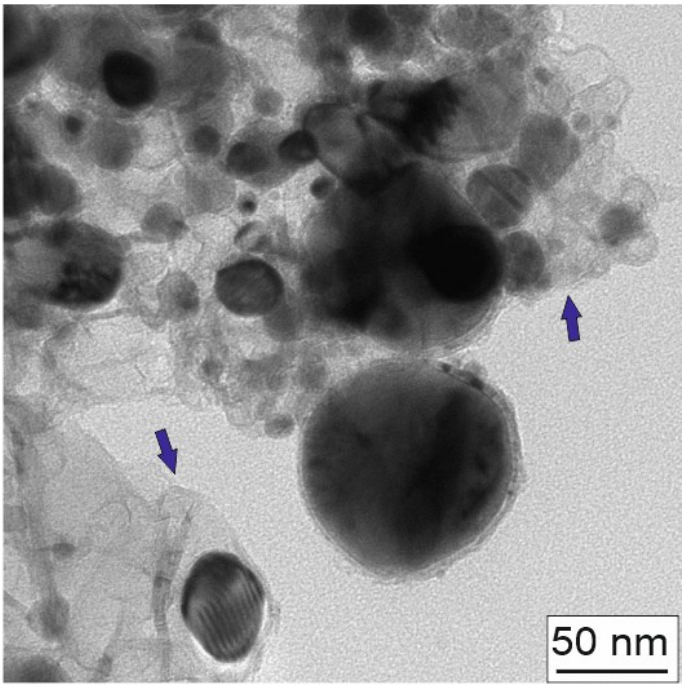


***Fig. S10.*** Representative TEM image of material **6**.

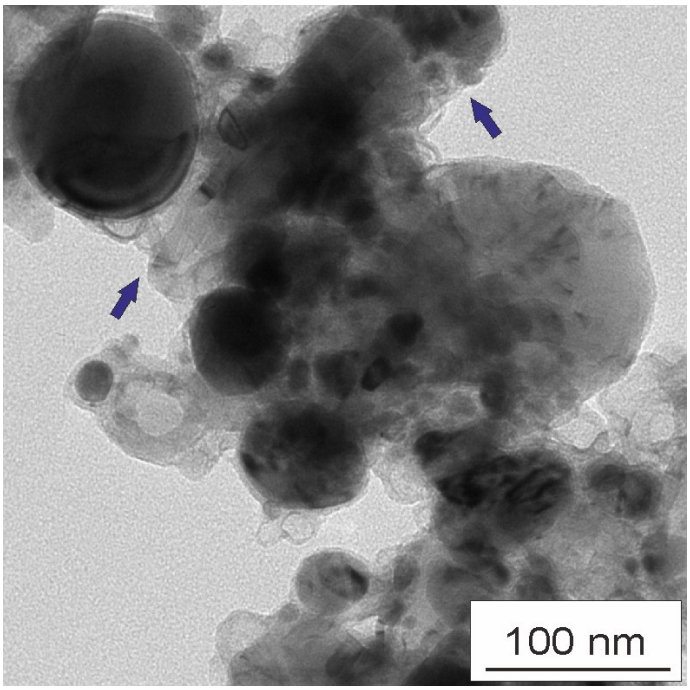


***Fig. S11.*** Representative TEM image of material **10**.

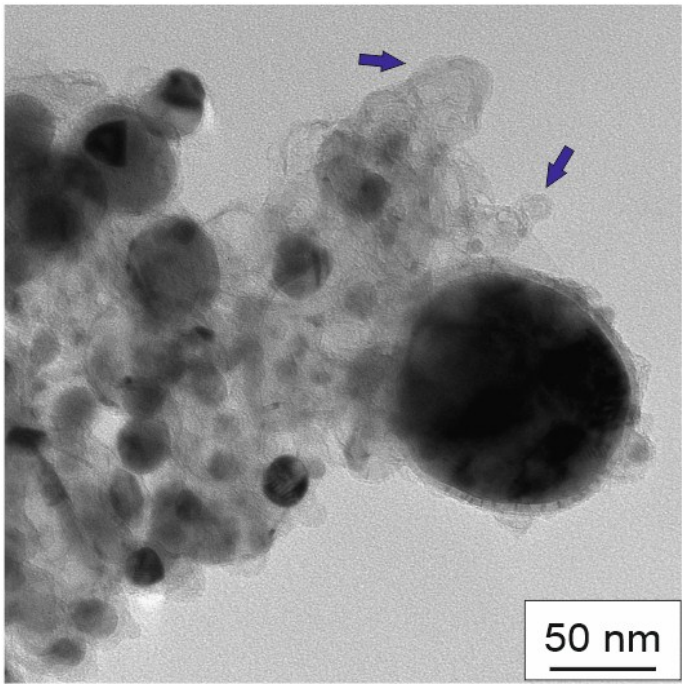


***Fig. S12.*** Representative TEM image of material **11**.

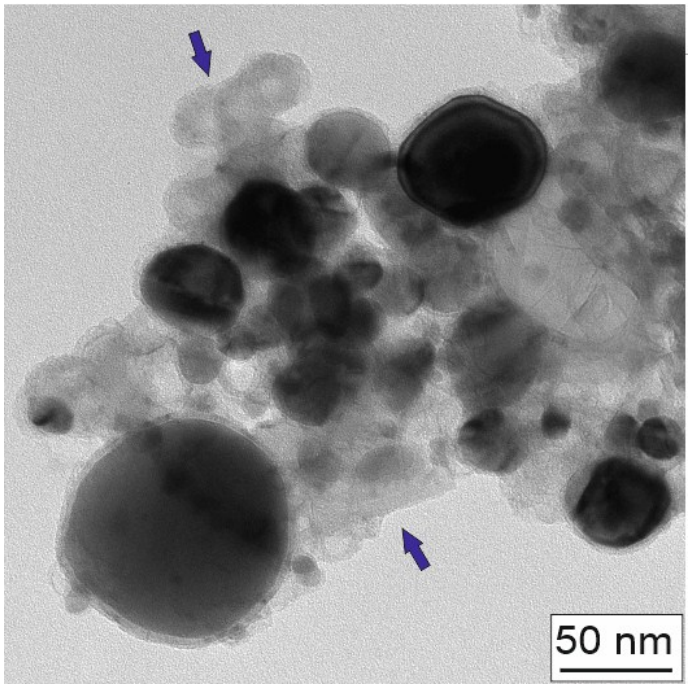


***Fig. S13*.** Representative TEM image of material **12**.

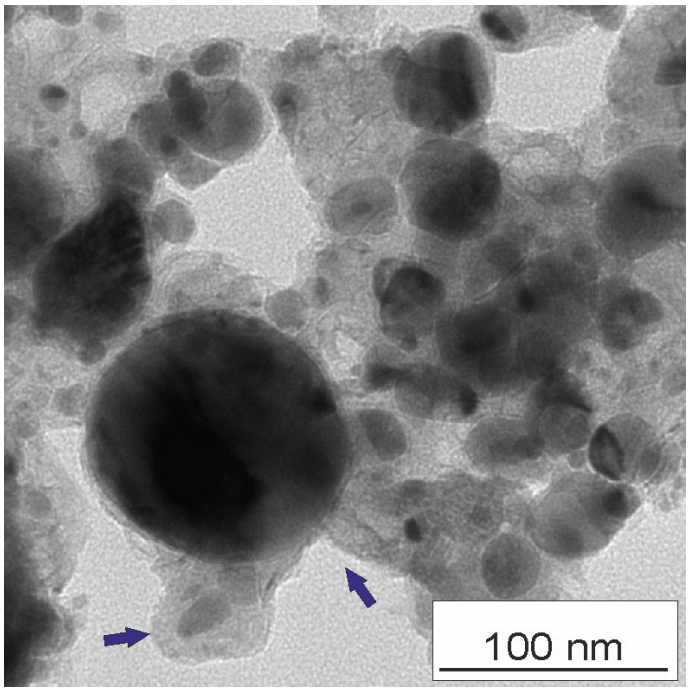


***Fig. S14*.** Representative TEM image of material **13**.

## 3. TGA measurements

Thermal decomposition and pyrolysis (under inert atmosphere) of sugars and their derivatives results in the formation of char. The char formation yield is different for various carbohydrates and depends on their chemical composition. The char formation yields for D-mannose oxime (20.0%)[1], D-galactose oxime (20.0%)[1], β-cyclodextrin (6.0%)[2] and glucosamine (12%)[3] were reported earlier. Char formation yield for D-mannose pentaacetate oxime (2.7%), 1,2:3,4-di-O-isopropylideno-β-D-galactopiranose oxime (0.9%) and chitosan (32.0%) was calculated from the TGA curves, which are presented below. The char formation yield of the reactant (nitrile oxide) used in synthesis of material **9** was evaluated to be 40.6%. The evaluation is based on thermodynamic calculations (Factsage 6.2 thermodynamic package). The TGA curve (in nitrogen) for material **1** is published elsewhere.[1]

For materials **1-7** and **9**, because of formation of char, which originates from the introduced sugar ligand, the functionalization yield was calculated as follows: $C = (WL_{500}-M)\cdot(100\%-CH)$, where C is the content of introduced sugar ligand [wt%], $WL_{500}$ is the observed weight loss up to 500°C, M is a content of moisture in the sample (weight loss up to 110°C), CH – char formation yield.

For material **8**, the content of the introduced organic moiety was calculated as follows: $C = (WL_{500}-M)$, because char is not formed from the decomposition of carboxylic moieties.

For materials **10-13** the weight loss from 110°C to 500°C consists of two components, namely the weight loss coming from the starting carbon material (material **8** or **9**) and the weight loss coming from the sugar ligand. The functionalization yield for materials **10-13** was therefore calculated as follows: $C = [(WL_{amide,500}-M_{amide})-(WL_{COOH,500}-M_{COOH})]\cdot(100\%-CH)$, where C is the content of introduced sugar ligand [wt%], $WL_{amide,500}$ is the observed weight loss for material **10-13** up to 500°C, $M_{amide}$ is a content of moisture for material **10-13** (weight loss up to 110°C), $WL_{COOH,500}$ is the observed weight loss for the reactant (material **8** or **9**) up

to 500°C, $M_{COOH}$ is a content of moisture for the starting carbon material (material **8** or **9**; weight loss up to 110°C), CH – char formation yield.

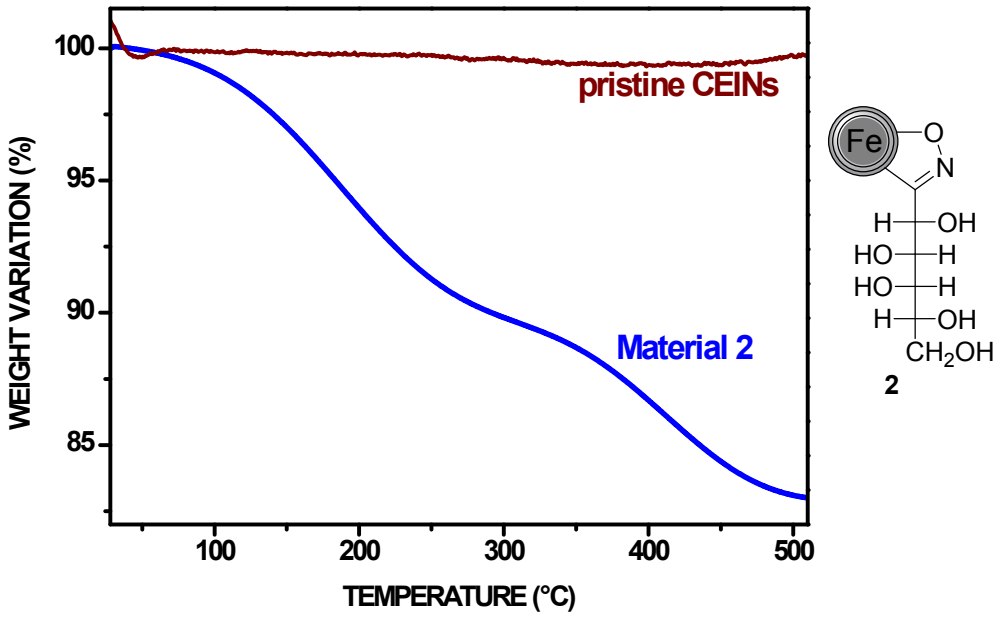


***Fig. S15.*** TGA curve (in nitrogen) for material **2**. TGA curve for pristine CEINs is also presented.

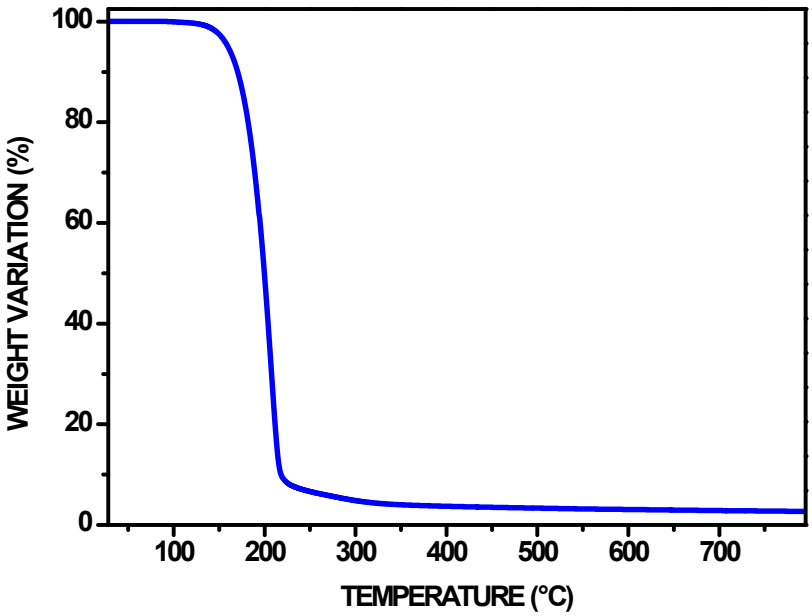


***Fig. S16.*** TGA curve (in nitrogen) for D-mannose pentaacetate oxime.

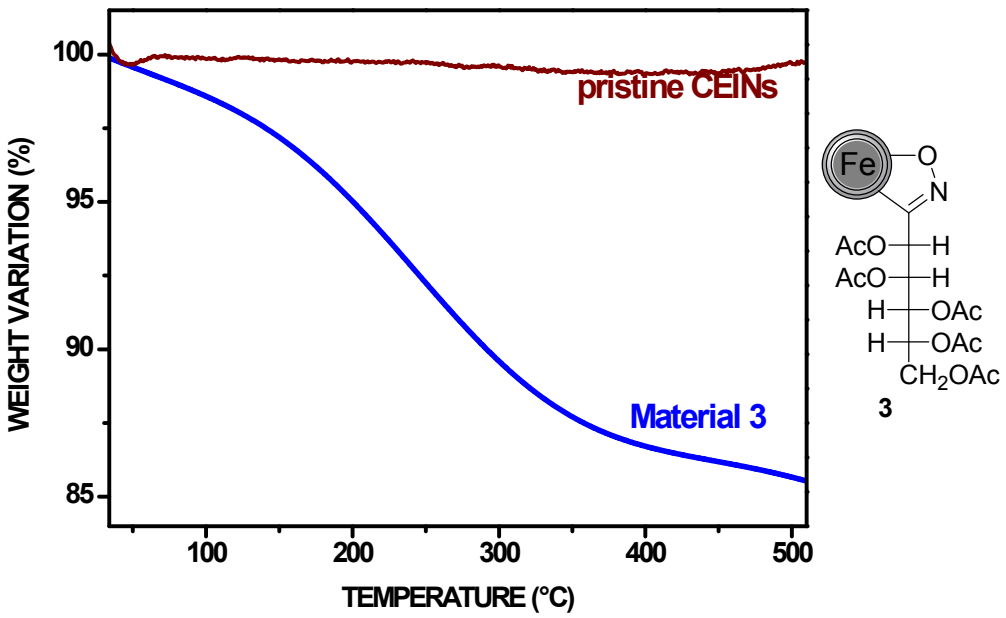


***Fig. S17.*** TGA curve (in nitrogen) for material **3**. TGA curve for pristine CEINs is also presented.

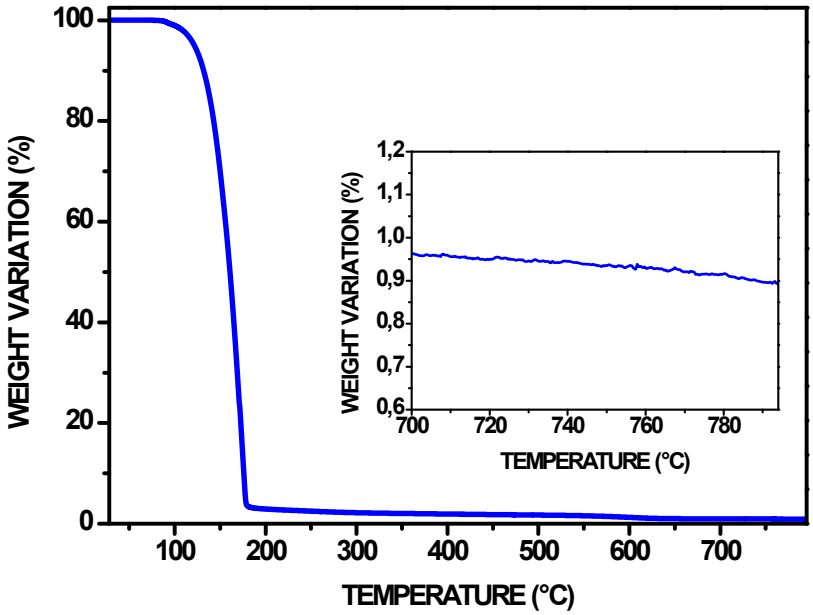


***Fig. S18.*** TGA curve (in nitrogen) for 1,2:3,4-di-*O*-isopropylidene-β-D-galactopiranose oxime. The inset of the TGA curve in the temperature range from 700 °C is presented.

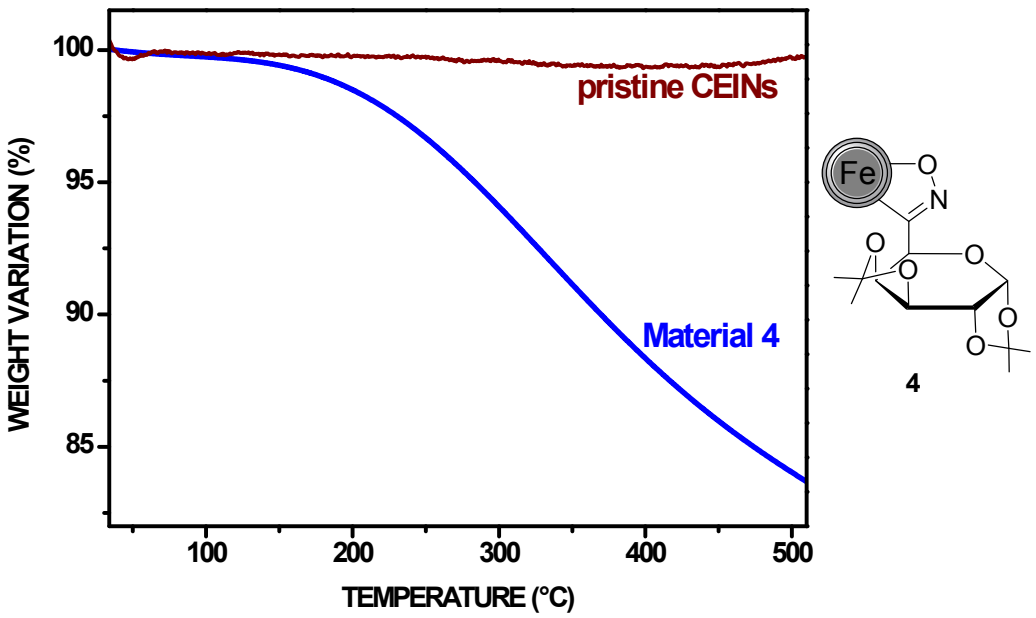


***Fig. S19.*** TGA curve (in nitrogen) for material **4**. TGA curve for pristine CEINs is also presented.

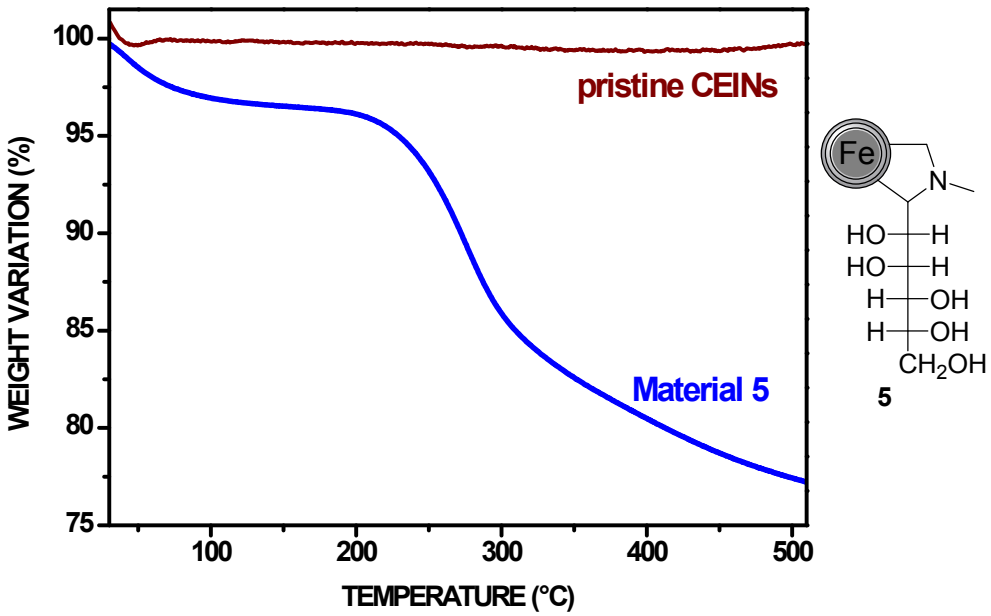


***Fig. S20.*** TGA curve (in nitrogen) for material **5**. TGA curve for pristine CEINs is also presented.

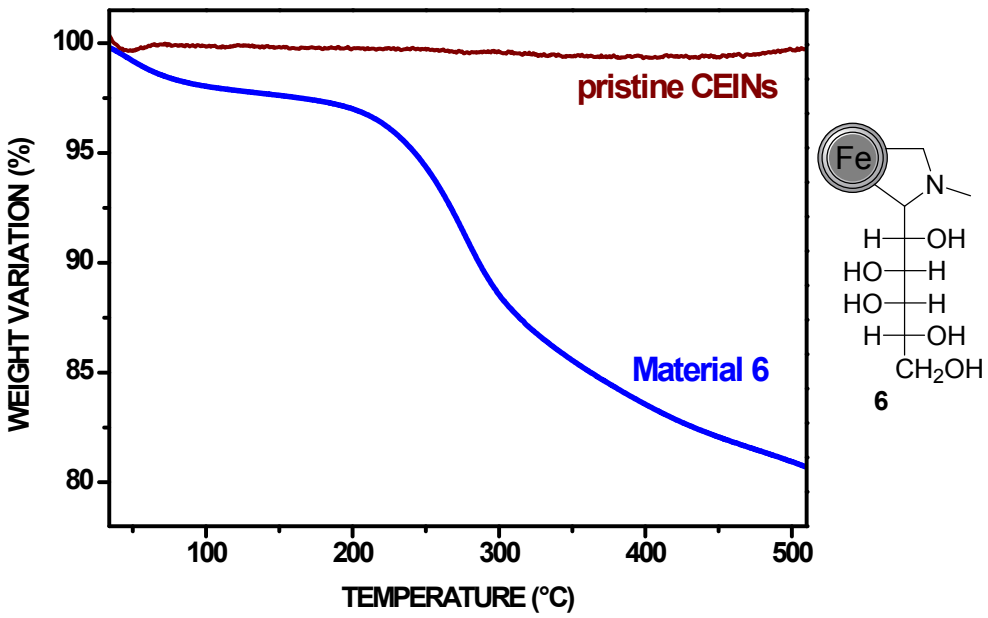


***Fig. S21.*** TGA curve (in nitrogen) for material **6**. TGA curve for pristine CEINs is also presented.

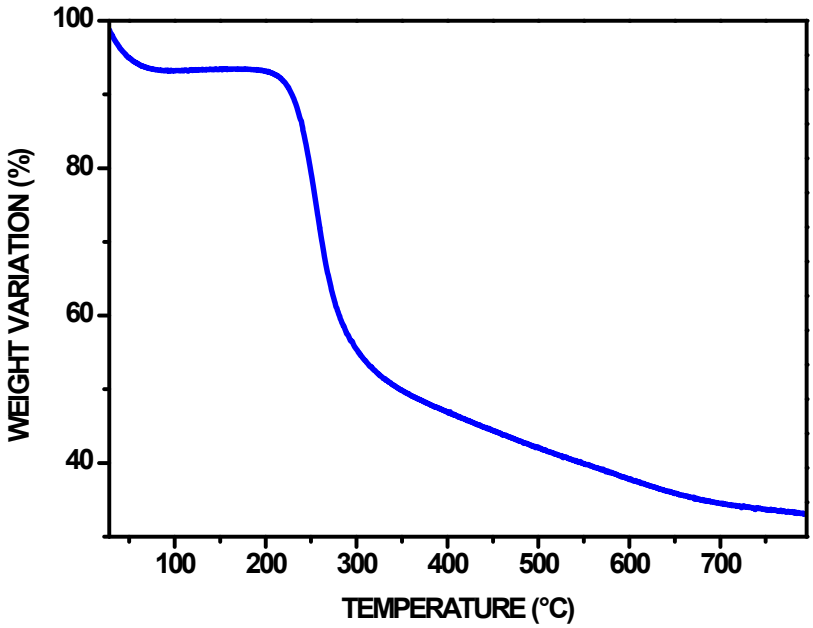


***Fig. S22.*** TGA curve (in nitrogen) for chitosan.

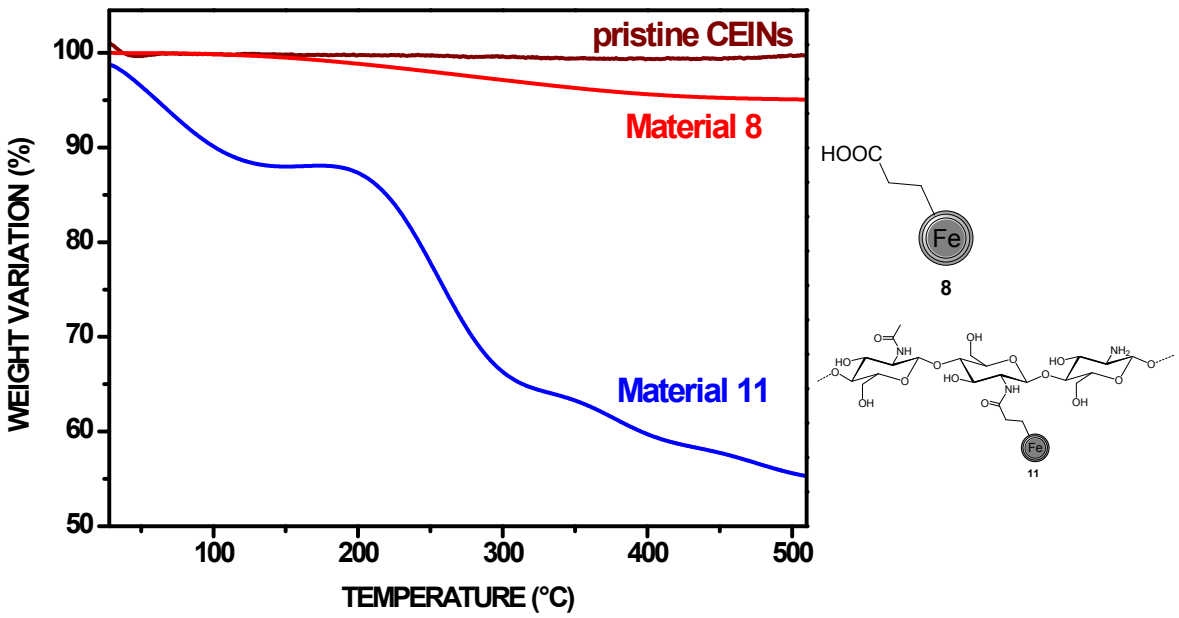


***Fig. S23.*** TGA curve (in nitrogen) for material **11**. TGA curves for pristine CEINs and CEINs-$(CH_2)_2$-COOH (**8**) are also presented.

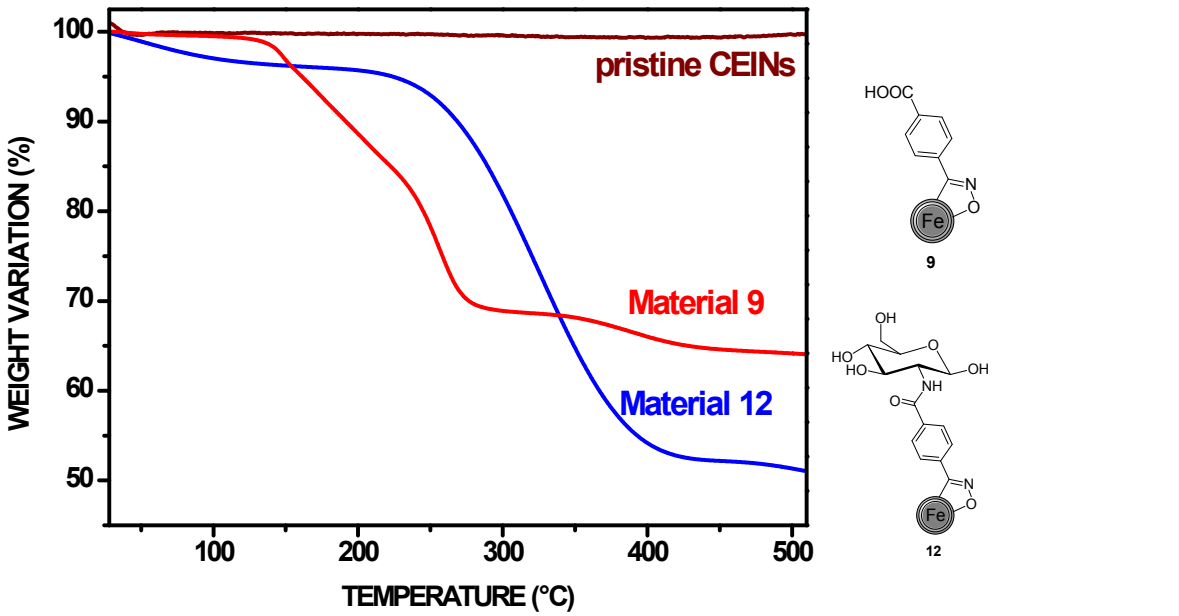


***Fig. S24.*** TGA curve (in nitrogen) for material **12**. TGA curves for pristine CEINs and CEINs-isoxazoline-COOH (**9**) are also presented.

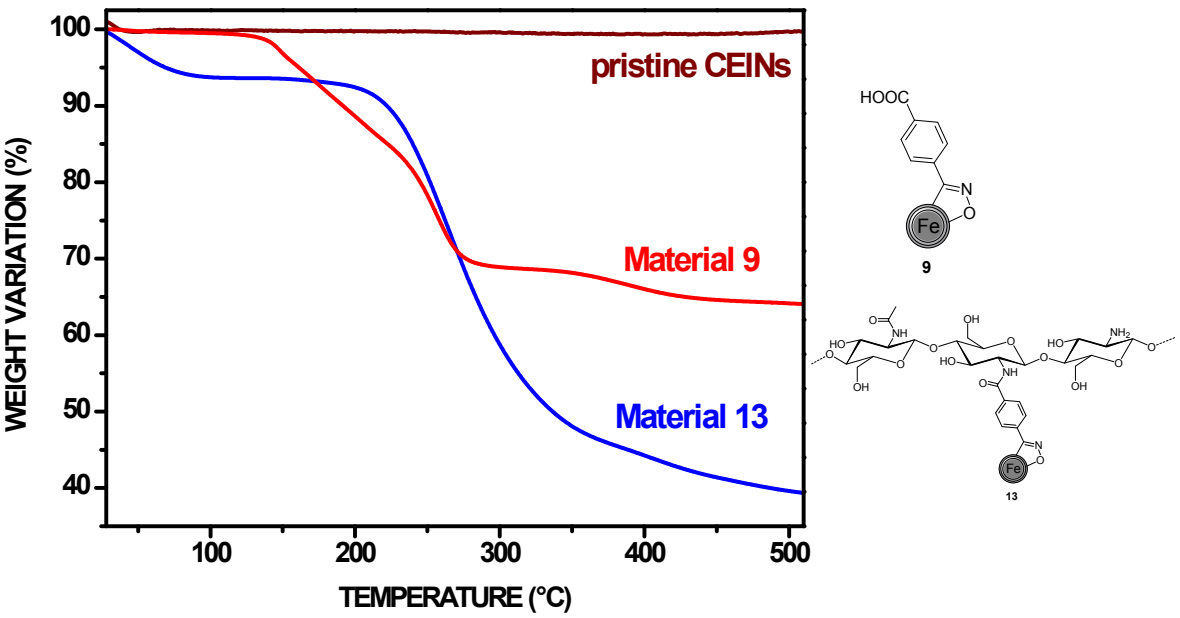


***Fig. S25.*** TGA curve (in nitrogen) for material **13**. TGA curves for pristine CEINs and CEINs-isoxazoline-COOH (**9**) are also presented.

## 4. Magnetic hysteresis loops

Magnetic hysteresis loops were acquired for each synthesized material.

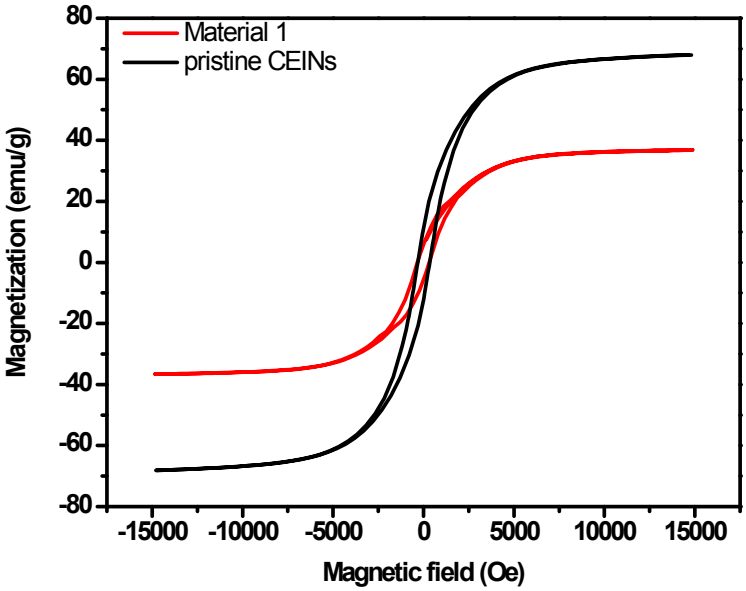


***Fig. S26.*** Magnetic hysteresis loop for material **1**. Magnetic hysteresis loop for pristine CEINs is also shown.

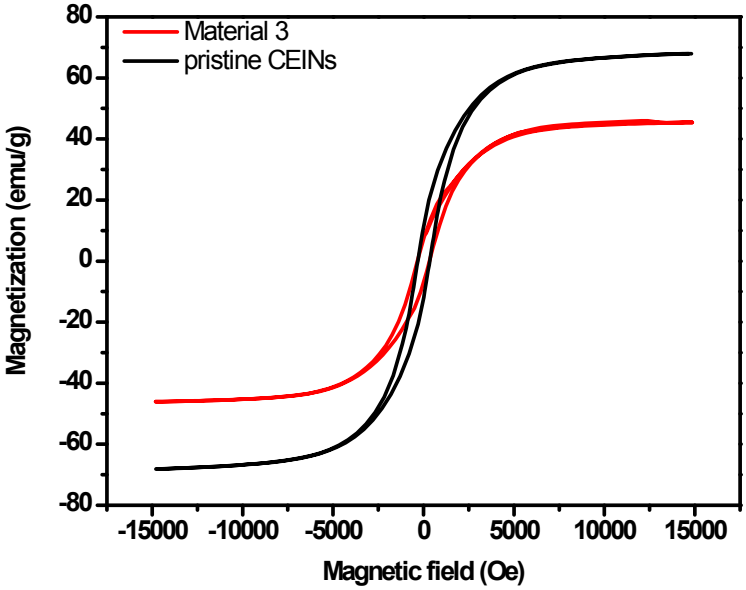


***Fig. S27.*** Magnetic hysteresis loop for material **3**. Magnetic hysteresis loop for pristine CEINs is also shown.

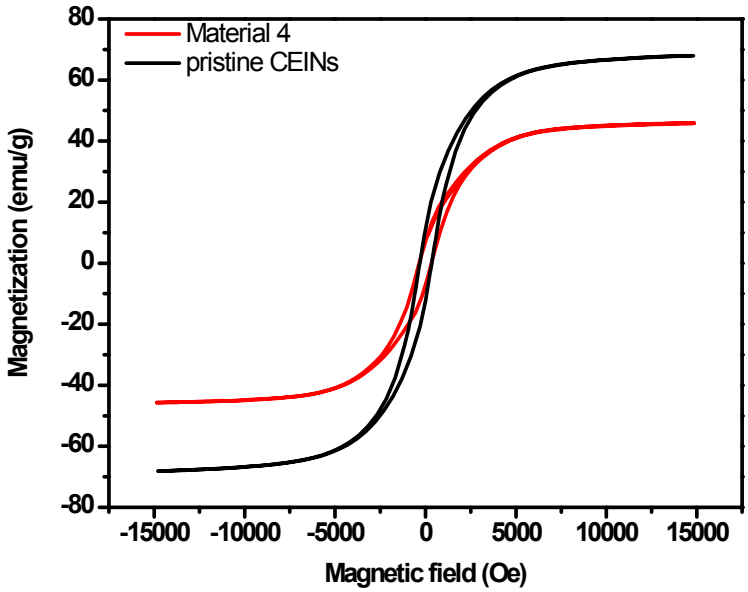


***Fig. S28.*** Magnetic hysteresis loop for material **4**. Magnetic hysteresis loop for pristine CEINs is also shown.

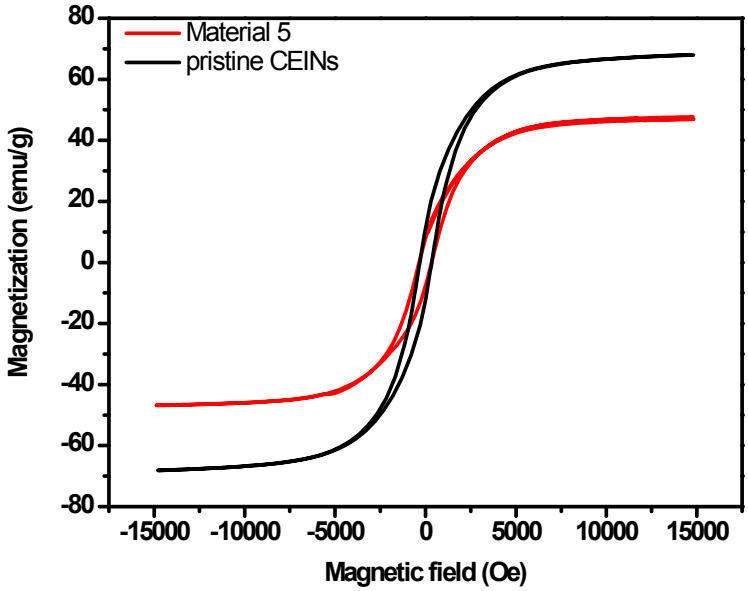


***Fig. S29.*** Magnetic hysteresis loop for material **5**. Magnetic hysteresis loop for pristine CEINs is also shown.

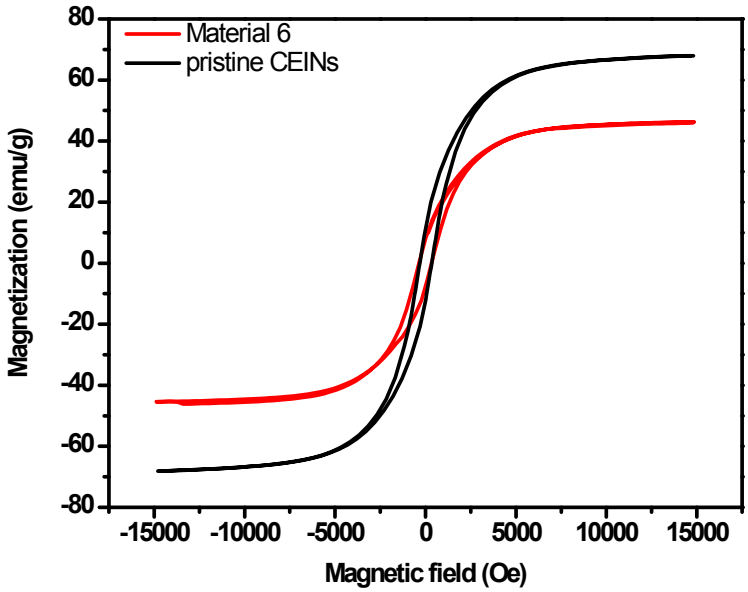


***Fig. S30.*** Magnetic hysteresis loop for material **6**. Magnetic hysteresis loop for pristine CEINs is also shown.

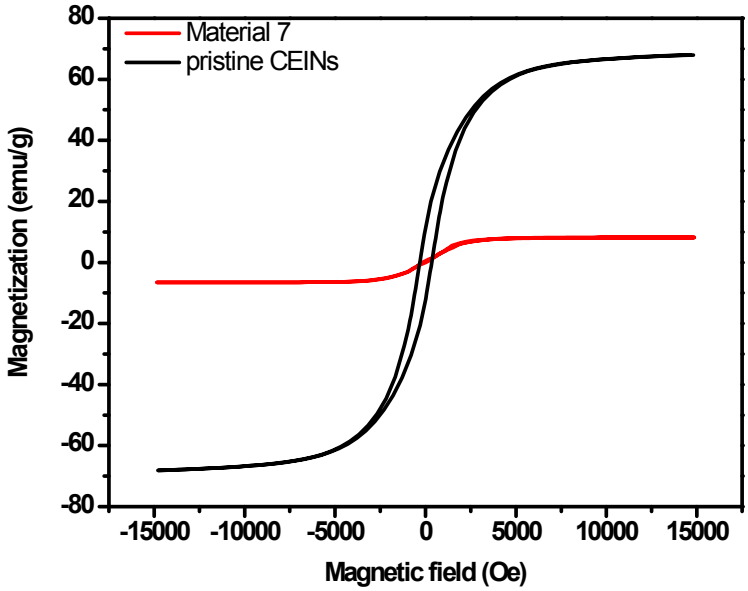


***Fig. S31.*** Magnetic hysteresis loop for material **7**. Magnetic hysteresis loop for pristine CEINs is also shown.

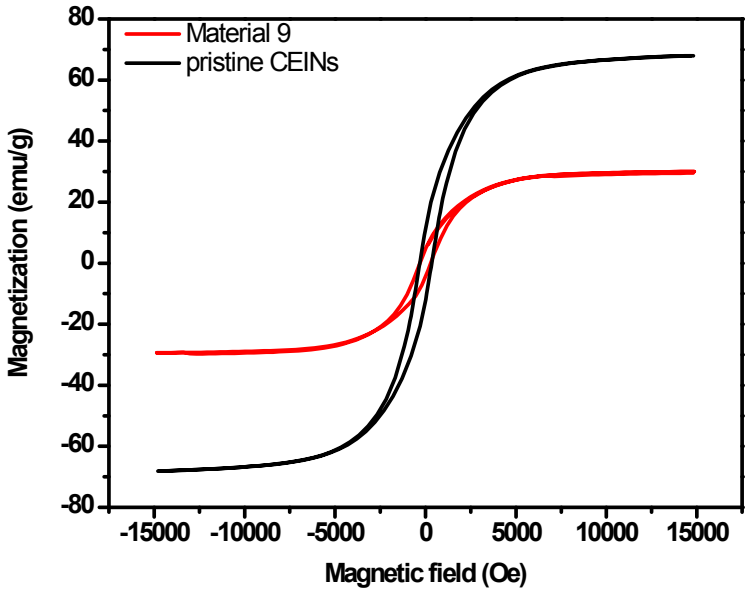


***Fig. S32.*** Magnetic hysteresis loop for material **9**. Magnetic hysteresis loop for pristine CEINs is also shown.

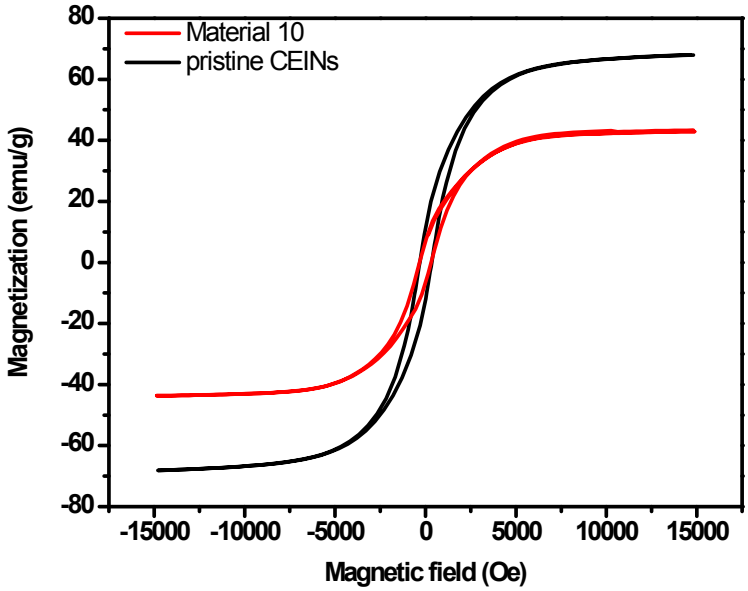


***Fig. S33.*** Magnetic hysteresis loop for material **10**. Magnetic hysteresis loop for pristine CEINs is also shown.

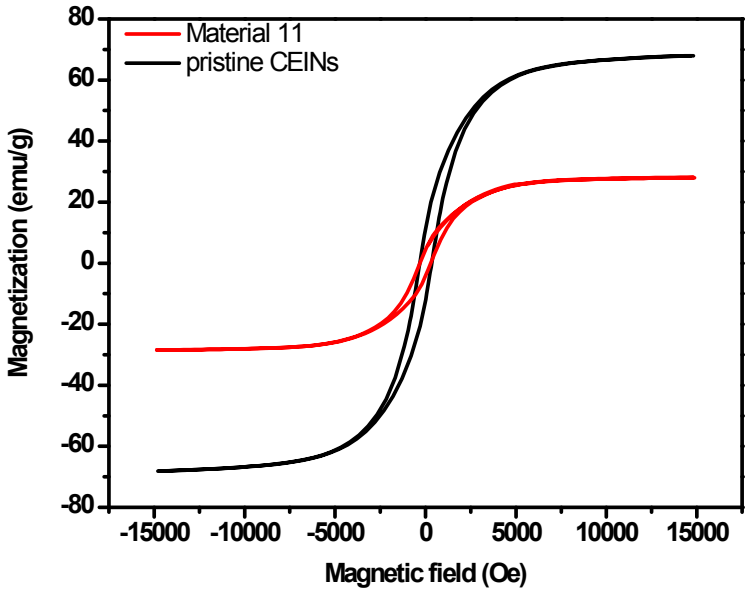


***Fig. S34.*** Magnetic hysteresis loop for material **11**. Magnetic hysteresis loop for pristine CEINs is also shown.

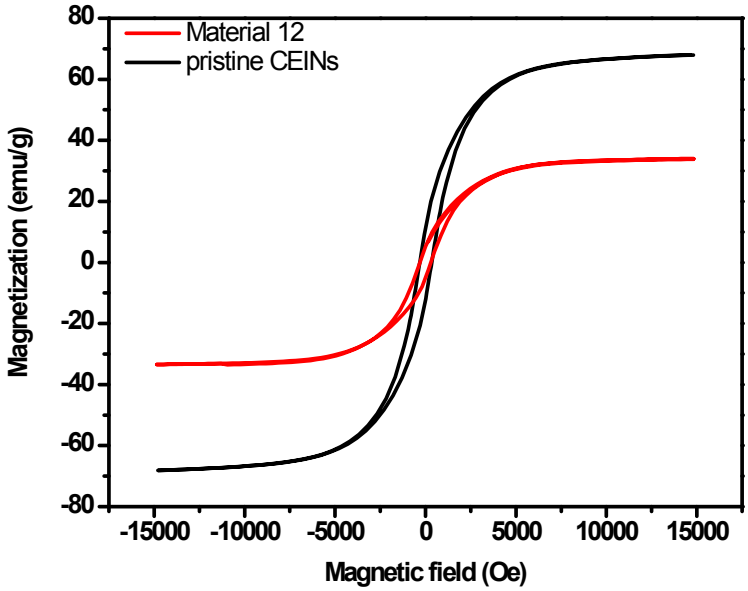


***Fig. S35.*** Magnetic hysteresis loop for material **12**. Magnetic hysteresis loop for pristine CEINs is also shown.

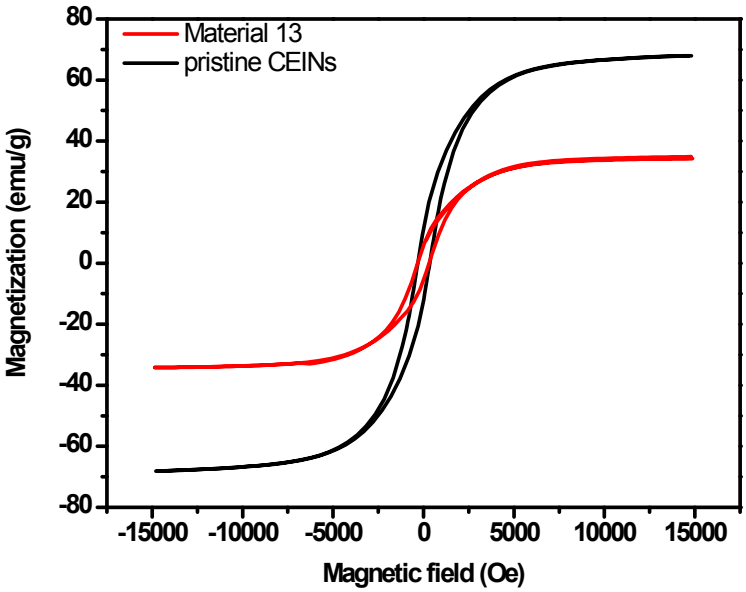


***Fig. S36.*** Magnetic hysteresis loop for material **13**. Magnetic hysteresis loop for pristine CEINs is also shown.

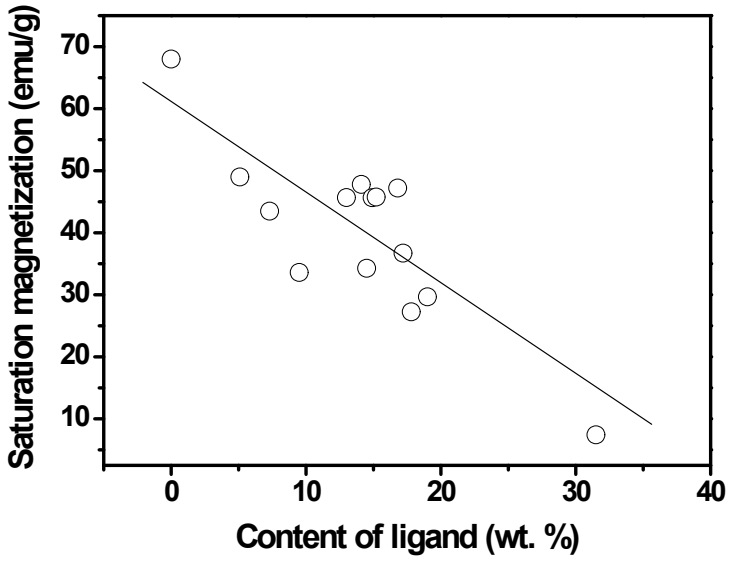


***Fig. S37.*** Saturation magnetization vs. content of introduced ligand.

## References


1 A. Kasprzak, M. Bystrzejewski, M. Koszytkowska-Stawinska and M. Poplawska, *Green Chem.*, 2017, **19**, 3510–3514.

2 P. Subramaniam, S. Mohamad and Y. Alias, *Int. J. Mol. Sci.*, 2010, **11**, 3675–3685.

3 F. A. A. Tirkistani, *Carbohydr. Polym.*, 1997, **34**, 329–334.